Ir-Catalyzed Atroposelective Desymmetrization of Heterobiaryls: Hydroarylation of Vinyl Ethers and Bicycloalkenes

Antonio Romero-Arenas,[†] Valentín Hornillos,[†,‡] Javier Iglesias-Sigüenza,[‡] Rosario Fernández,*[,‡] Joaquín López-Serrano,*[,§] Abel Ros,*[,†,‡] José M. Lassaletta*[,†].

[†]Instituto de Investigaciones Químicas (CSIC-US) and Centro de Innovación en Química Avanzada (ORFEO–CINQA), Avda. Américo Vespucio, 49, 41092 Sevilla, Spain

[§]Instituto de Investigaciones Químicas (CSIC-US). Departamento de Química Inorgánica and Centro de Innovaciones Química Avanzada (ORFEO-CINQA). Avda. Américo Vespucio, 49,41092 Sevilla, Spain

[‡]Departamento de Química Orgánica, Universidad de Sevilla and Centro de Innovación en Química Avanzada (ORFEO–CINQA), C/Prof. García González, 1, 41012 Sevilla, Spain

ABSTRACT: A highly regio, diastereo- and enantioselective, scalable Ir-catalyzed hydroarylation of electron rich acyclic and tensioned cyclic olefins with heterobiaryls is described. The reaction of acyclic vinyl ethers, dihydrofuran and norbornenes with a variety of aryl isoquinoline, quinazoline, and picoline derivatives takes place with simultaneous installation of central and axial chirality, reaching complete *branched/linear* or *exo/endo* ratios and excellent diastereo- and enantiomeric excesses when *in situ* formed [Ir^I/Tol-SDP] or [Ir^I/Tol-BINAP] complexes are used as the catalysts. Kinetic isotope effect (KIE) analyses and a comprehensive computational study suggest that, despite fast double bond migratory insertion into Ir-H, the reaction proceeds through a modified Chalk-Harrod mechanism, starting with selectivity-determining insertion into Ir-C_{Aryl}. The regioselectivity is controlled by the electron donating alkoxy group, whereas diastereo- and enantioselectivity have a complex origin, that depend on the relative orientation of the alkoxy group and the establishment of adequate π-π interactions between the biaryl and the phosphine.

1. INTRODUCTION

The asymmetric synthesis of axially chiral compounds has attracted a special interest because axial chirality is a prevalent motif in many natural products and biologically active molecules,[1] and constitutes an important scaffold for the design of chiral ligands and organocatalysts with countless applications in asymmetric catalysis.[2] Consequently, the number of reports describing methodologies for their catalytic atroposelective synthesis has been steadily increasing in recent years. The reported methods are mainly based on direct cross or oxidative coupling reactions,[3] [2+2+2] cycloadditions,[4] organocatalytic approaches,[5] and the most recently described DKR-type strategies.[6] Most of these approaches, however, fail for the more challenging synthesis of axially chiral *heterobiaryl* derivatives,[7] and the development of alternative approaches remains as a relevant synthetic challenge.

In this regard, our group has developed a dynamic kinetic asymmetric transformation (DYKAT) strategy that was first applied to a *Suzuki–Miyaura* reaction and later extended to several C–C, C–P and C–N cross-coupling reactions.[8] As a limitation, however, this methodology requires relatively elaborated racemic heterobiaryl sulfonates/bromides as starting materials. A more appealing strategy exploits the *ortho*-directing effect of the heterobiaryl N atom to perform regioselective asymmetric C–H functionalization reactions (Scheme 1A). There is a plethora of catalysts based on different transition metals that have been used for the functionalization of 2-phenylpryridine and related heterobiaryls.[9] A closer analysis, however, reveals that the vast majority of these systems are not useful to our purpose. First, high temperatures are usually required, compromising the configurational lability of the products. Second, these reactions are highly sensitive to steric factors: the reactivity dramatically drops for substrates bearing substituents at positions *ortho* to the aryl-hetaryl bond, presumably for the destabilization of the cyclometalated intermediates. Nevertheless, a few remarkable exceptions, enabled by very efficient catalysts, are known: *a*) The pioneering Rh-catalyzed ethylene hydroarylation by Murai and co-workers[10] (Scheme 1B), yielding ethyl-substituted heterobiaryls with moderate yields and enantioselectivities. *b*) A Rh-catalyzed dehydrogenative Heck coupling using Cramer's Cp ligands[11] or Cp ligands based on 1,1′-spirobiindane ligands[12] (Scheme 1C). In both cases, aryl benzo[*h*]isoquinoline substrates are required to reach high enantioselectivities. *c*) A recently reported Rh-catalyzed C–H Arylation[13] (Scheme 1D).

Aiming to develop a C–H functionalization protocol feasible under mild conditions, hence compatible with the integrity of the stereogenic axis, we also developed time ago a strategy to perform N-directed borylation of heterobiaryls[14] (Scheme 1E). The efficiency of the method allowed to perform borylation of 1-(naphth-1-yl)isoquinoline and analogues to afford versatile heterobiaryl boronates which, unfortunately, proved to be configurationally labile, presumably due to the easy atropisomerization *via* N→B internal *ate* complexes as intermediates. This precedent, however, underlines the

Scheme 1. Heterobiaryl Synthesis *via* C–H Activation.

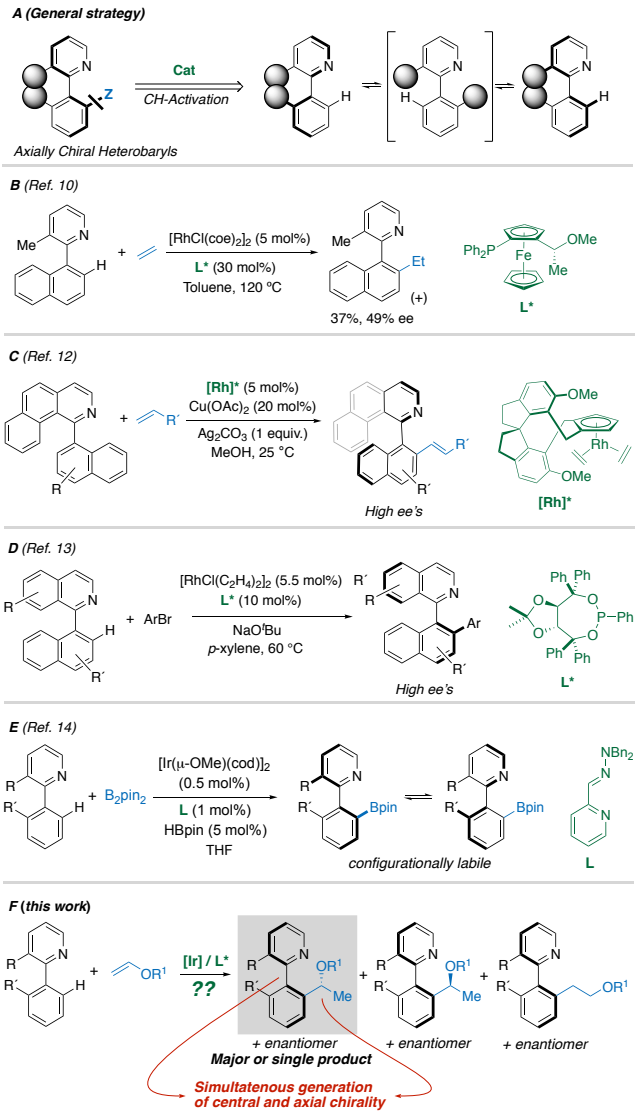

suitability of Ir catalyst to perform the challenging, regioselective C–H activation of *ortho,ortho'*-disubstituted heterobiaryls, paving the way to alternative atroposelective transformations. Inspired also in the Ir-catalyzed asymmetric hydroarylation of vinyl ethers developed by Nishimura and co-workers,[15] we decided to explore the atroposelective desymmetrization of heterobiaryls *via* Ir-catalyzed hydroarylation of olefin/vinyl ethers (Scheme 1F).

A priori, the designed transformation represents a significant synthetic challenge, since a number of difficulties have to be taken into account: (1) the catalysts must be highly efficient to enable formation of tensioned cyclic intermediates; (2) after the C–H activation step, an Ir^{III} octahedral intermediate with chirality at the metal center is generated, greatly increasing the number of possible stereoisomers; (3) the olefin can be inserted on the external or internal position during the migratory insertion step, generating the branched or linear isomer after reductive elimination; (4) the catalyst must control the generation of two stereogenic elements (stereogenic axis in the heterobiaryl and stereocenter at C1 from the olefin). Summarizing, the chiral ligand will be required to provide a high reactivity while performing an exquisite control of *branched/linear*, diastereo- and enantioselectivity to afford satisfactory results.

2. RESULTS AND DISCUSSION

Reaction optimization. Preliminary studies were carried out using the coupling between *n*-butyl vinyl ether **1a** and naphthylisoquinoline **2** as the model reaction, using 2.5 mol% $[IrCl(cod)_2]$/6 mol% BINAP (**L1**) and 10 mol% $NaBAr^F$ (Ar^F= 3,5-CF_3-C_6H_3) as the catalyst system (Table 1). Initially, toluene was used as a non-coordinating solvent in reactions with 2 equiv. of **1a** (entry 1), affording the desired product (S_a,*R*)-**7** with a complete *branched/linear* selectivity, excellent [(S_a,*R*)-**7**/(S_a,*S*)-**7**)] diastereomeric ratio, and a promising 85% ee, although a low conversions was observed. Increasing the amount of **1a** to 5 equiv. improved the conversion,

Table 1. Screening of Reaction Conditions and Ligands.[a]

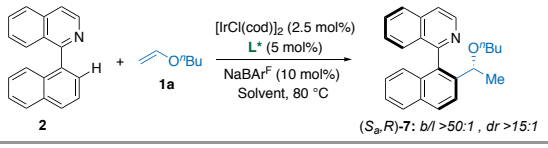

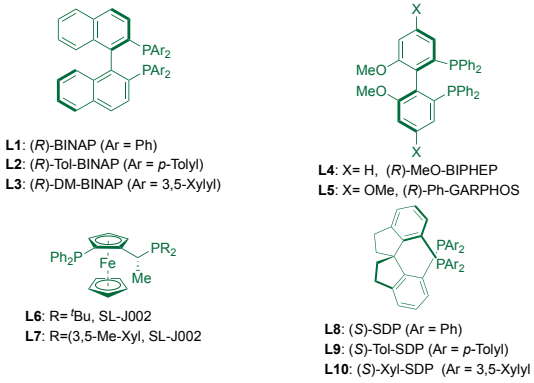

Entry	Ligand	Solvent	Conv (%)[b]	Ee[c]
1[d]	**L1**	Toluene	25	85
2	**L1**	Toluene	50	84
3	**L1**	THF	80	84
4	**L1**	DME	50	83
5	**L1**	DCE	80	83
6	**L1**	Dioxane	>95	83
7	**L2**	Dioxane	>95	90
8	**L3**	Dioxane	90	84
9	**L4**	Dioxane	85	33
10	**L5**	Dioxane	30	34
11	**L6**	Dioxane	10	45
12	**L7**	Dioxane	10	12
13	**L8**	Dioxane	65	87
14	**L9**	Dioxane	>95	93
15	**L10**	Dioxane	60	95

[a] Reactions performed on a 0.1 mmol scale using anhydrous solvent (1 mL/0.1 mmol **2**) and 5 equiv. of **1a**, for a 24 h period at 80 °C. [b] Determined by ^{1}H NMR spectroscopy of the crude reaction mixture. The *branched/linear* ratio and the diastereoselectivity [(*Sa,R*)-**7**/(*Sa,S*)-**7**] were also determined by ^{1}H NMR on the reaction crude, being >20:1 and >20:1, respectively, in all cases. [c] Determined by chiral HPLC analysis. [d] 2 equiv. of **1a** were used.

but it still remained unsatisfactory (entry 2), presumably due to the polymerization of the starting vinyl ether **1a**.[15] Additional experiments were performed to explore the effect of the solvent in controlling the undesired polymerization (entries 3-6). From these experiments, coordinating anhydrous 1,4-dioxane proved to be the best option, affording full conversion while maintaining high levels of diastereo- and enantioselectivity (entry 6). Under these conditions, other chiral *P,P* ligands were tested. Similar reactivities were observed with substituted BINAP derivatives **L2** and **L3** (entries 7 and 8), although a better enantioselectivity was achieved with *Tol*-BINAP **L2** (entry 7), leading to the desired product (S_a,*R*)-**7** with perfect *dr* (>20:1) and 90% ee. Disappointing results were observed with other axially chiral ligands such as *MeO*-BIPHEP **L4** (entry 9) and *Ph*-GARPHOS **L5** (entry 10). On the other hand, Josiphos-type ligands **L6** and **L7** were unproductive (entries 11 and 12). Finally, spiro diphosphines (SDP)[16] such as **L8–L10** (entries 13–15) afforded the best enantioselectivity levels. In particular, (*S*)-*Tol*-SDP **L9** provided the best reactivity/selectivity balance, affording full conversion and a 93% ee (entry 14).

Reaction Scope. With the optimized conditions in hands [*6 mol% **L9**/2.5 mol% [IrCl(cod)]$_2$, 10 mol% NaBAr^F, 5 equiv. **1a**, 1,4-dioxane (1 mL/0.1 mmol **2**)*], the desymmetrization methodology was successfully applied to the hydroarylation of other vinyl ethers **1b-f** with different heterobiaryls **3–6** (Table 2). The reaction worked well at 80 °C with *n*-butyl vinyl ether **1a** and heterobiaryls **2–5**, affording exclusively the corresponding branched products (S_a,*R*)- **7–10a** after 24 h in excellent yields (88-95%) and dr's (>20:1), along with very high ee's (up to 98%). The extension to other acyclic vinyl

Table 2. Scope of Hydroarylation Reactions with Acyclic Vinyl Ethers.[a]

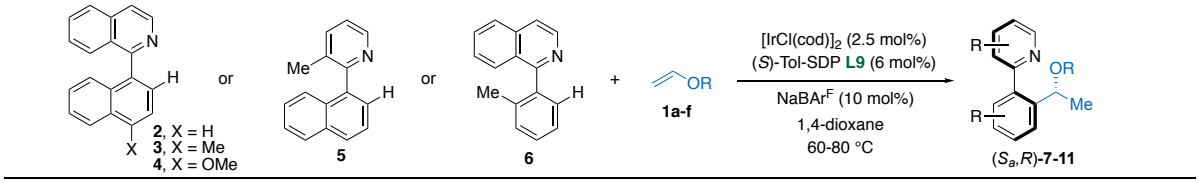

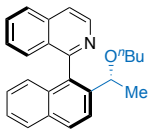
(S_a,*R*)-**7a**: 95%, dr >20:1, 94% ee

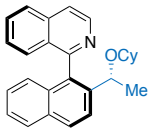
(S_a,*R*)-**7b**: 87%, dr >20:1, 96% ee

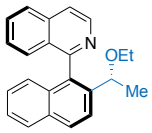
(S_a,*R*)-**7c**:[b] 89%, dr 13:1, 93% ee

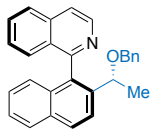
(S_a,*R*)-**7d**: 70%, dr >20:1, 97% ee

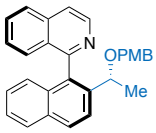
(S_a,*R*)-**7e**: 66%, dr >20:1, 91% ee

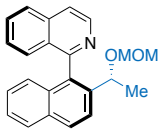
(S_a,*R*)-**7f**:[c] 70%, dr >20:1, 97% ee

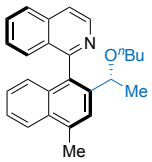
(S_a,*R*)-**8a**: 92%, dr >20:1, 95% ee

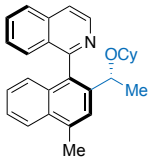
(S_a,*R*)-**8b**: 89%, dr >20:1, 98% ee

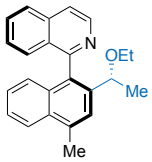
(S_a,*R*)-**8c**:[b] 94%, dr 13:1, 86% ee

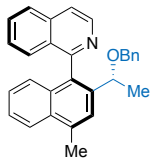
(S_a,*R*)-**8d**: 72%, dr >20:1, 96% ee

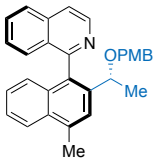
(S_a,*R*)-**8e**: 44%, dr >20:1, 98% ee

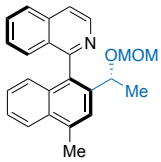
(S_a,*R*)-**8f**:[c] 76%, dr >20:1, 98% ee

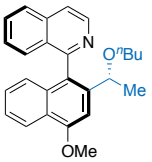
(S_a,*R*)-**9a**: 91%, dr >20:1, 80% ee

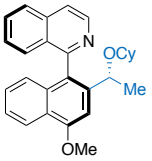
(S_a,*R*)-**9b**: 92%, dr >20:1, 91% ee[d]

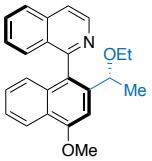
(S_a,*R*)-**9c**:[b] 92%, dr 10:1, 53% ee

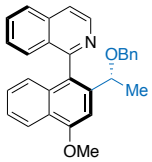
(S_a,*R*)-**9d**: 91%, dr >20:1, 91% ee

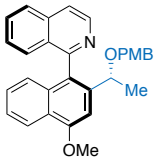
(S_a,*R*)-**9e**: 51%, dr >20:1, 89% ee

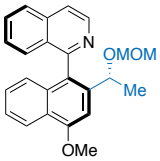
(S_a,*R*)-**9f**:[c] 90%, dr >20:1, 89% ee

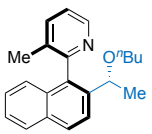
(S_a,*R*)-**10a**: 94%, dr >20:1, 98% ee

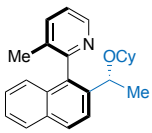
(S_a,*R*)-**10b**: 87%, dr >20:1, 98% ee

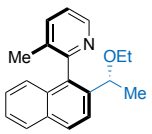
(S_a,*R*)-**10c**:[b] 96%, dr 15:1, 96% ee

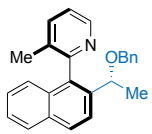
(S_a,*R*)-**10d**: 45%, dr >20:1, 99% ee

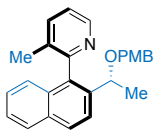
(S_a,*R*)-**10e**: 33%, dr >20:1, 99% ee

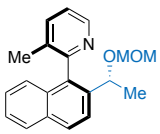
(S_a,*R*)-**10f**:[c] 79%, dr >20:1, 99% ee

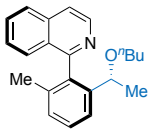
(S_a,*R*)-**11a**:[b] 88%, dr >20:1, 98% ee

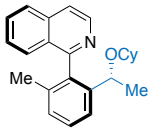
(S_a,*R*)-**11b**:[b] 78%, dr >20:1, 98% ee

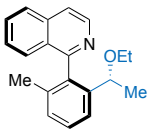
(S_a,*R*)-**11c**:[b] 65%, dr >20:1, 95% ee

[a] Reactions performed at 0.1 mmol scale in anhydrous 1,4-dioxane (1 mL/0.1 mmol **2–6**) with 5 equiv. of **1a–f** for a 24 h period at 80 °C. Isolated yields refer to major isomer after chromatography. Dr's were determined by ^{1}H NMR in the crude reaction mixtures. Ee's were determined by chiral HPLC analysis. [b] 20 equiv. of **1c** were used at 60 °C for 48 h. [c] 20 equiv. of **1d-f** were used at 80 °C for 24 h. [d] >99% ee after a single crystallization.

ethers such as **1b–c** afforded the desired heterobiaryls **7–10b–c** in moderate to excellent yields while maintaining high levels of diastereo- and enantioselectivity. Substituted acyclic vinyl ethers (e.g. the simplest ethyl-1-propenyl ether) were unreactive, even under forcing conditions. This limitation is attributed to the considerable steric crowding introduced by the heterobiaryl fragment in the hexacoordinate key intermediates and transition states (see mechanism discussion below). The absolute configuration of (S_a,*R*)-**9b** was determined by single-crystal X-ray diffraction analysis (Figure 1), while that of other products **7–10** was assigned by analogy. The reactions with ethyl vinyl ether **1c** were carried at 60 °C for 48 h and with a larger excess of reagent due to its higher volatility (bp 33 °C). Besides, the lower steric hindrance exerted by the ethyl group in comparison with the *n*-Bu or Cy groups on vinyl ethers **1a–b** caused the diastereoselectivity to drop from >20:1 to >9:1 (see the mechanism discussion below). In the case of the less reactive heterobiaryl **6**, the consumption of the vinyl ether **1a** by a competitive polymerization process was faster at 80 °C than the hydroarylation reaction itself. Fortunately, the expected axially chiral products **11a–c** were obtained in moderate to excellent (65%-88%) yields, and with very high enantioselectivities (96–99% ee) by performing the hydroarylation reaction at 60 °C and with a larger excess (20 equiv.) of **1a–c.**

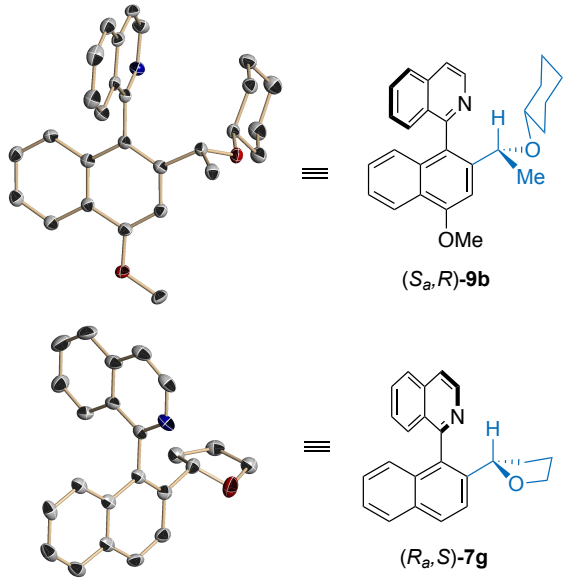

Figure 1. X-ray structures of (S_a,*R*)-**9b** and (R_a,*S*)-**7g**. Thermal ellipsoids drawn at 50% probability. H atoms are omitted for clarity.

Trimethylsilyl vinyl ether, a reagent envisaged to obtain deprotected secondary alcohols after removal of the trimethylsilyl group, did not react with **2,** even under forcing conditions. This lack of reactivity is most likely due to the higher steric bulk of the silyl group. As an alternative, the hydroarylation reaction was performed with vinyl ethers **1d–f**, which contain also removable groups such as Bn, PMB (*p*-methoxybenzyl), or MOM (methoxymethyl). The behavior of benzyl vinyl ether **1d** was similar to that of the model regent **1a**: using 5 equiv. of **1d** at 80 °C, the desired products **7d–10d** were obtained in moderate to excellent 45–91% yields, dr's higher than 20:1, and ee's up to 99%. Likewise, the hydroarylation reaction with PMB and MOM vinyl ethers **1e** and**1f** afforded the corresponding products **7-10e,f** with excellent levels

Table 3. Hydroarylation of 2,3-Dihydrofurane 1g.[a]

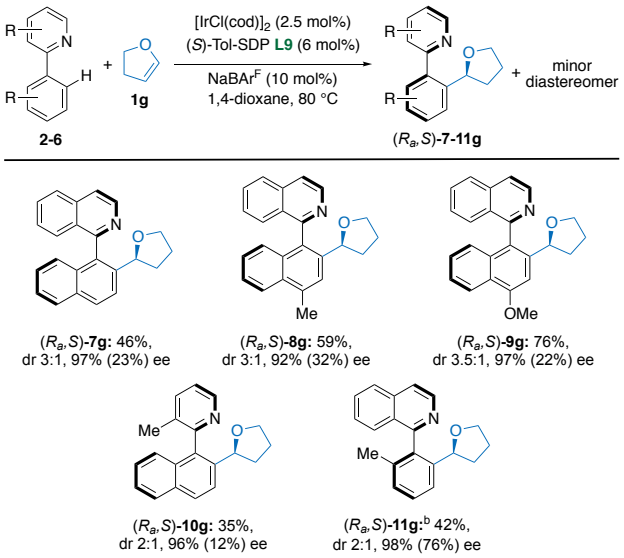

[a]Reactions performed on a 0.1 mmol scale (1 mL/0.1 mmol **2-6**) and 10 equiv. of vinyl ether **1g** , for a 24h period at 80 °C. Isolated yields of pure major isomer after chromatography. Diastereoisomeric ratios (dr) were determined by ^{1}H NMR in the crude reaction mixtures. Ee's were determined by chiral HPLC analysis. Values in brackets correspond to the minor diastereomer, whose absolute configuration was not determined.[b] 20 equiv. of vinyl ether **1f** were used.

of regio-, diastereo-, and enantioselectivity, although a larger excess of reagent was necessary to reach moderate to excellent (33–90%) yields. As an exception, methoxy-substituted heterobiaryl **4**, showed lower enantioselectivities in some cases.[16]

The methodology could be extended to a cyclic electron-rich alkene such as 2,3-dihydrofurane **1g** (Table 3), although a significant drop in the diastereoselectivity (dr ~3:1) was observed. Both diastereoisomers of **7g-11g** could be separated by column chromatography, affording the major diastereoisomer (R_a,*S*)-**7-11g** in moderate to good yields (35% to 76%) with enantioselectivities higher than 92% ee. Single-crystal X-ray diffraction analysis of (R_a,*S*)-**7g** unequivocally confirmed its absolute configuration(Figure 1) which, surprisingly, is opposite to that observed for the acyclic products **7-11a–f**. For a plausible explanation of this unexpected observation, see the mechanism discussion below. Less strained 3,4-dihydro-2H-pyran proved to be unreactive, but the atroposelective hydroarylation protocol could alternatively be extended to tensioned cyclic alkenes such as norbornene **1h** and functionalized derivative **1i** (Table 4). Using in this case [IrCl(cod)$_2$]/(*R*)-Tol-BINAP **L2** as the catalyst (see the SI for the optimization of the reaction conditions), these substrates readily reacted with heterobiaryls **2–6,12-14** to afford the desired adducts **7–11,15-17h** in moderate to near quantitative yields, with enantioselectivities up to 99% ee and as a single *exo* diastereomer. The *exo* selectivity, and the absolute configuration of the products, could be again confirmed by X-ray diffraction analysis of (R_a,*R*,*R*,*S*) **16h** (Figure 2). Assuming an uniform reaction pathway for the rest of the products, the same absolute configuration was assigned to analogues (R_a,*R*,*R*,*S*) **7-11,15,17h**, while the absolute configuration of **i** series major isomers was assigned to be (R_a,*R*,*R*,*S*,*R*,*S*)-**7-10i,15i,16i**. The hydroarylation reaction of **1h** with **2** could be

Table 4. Hydroarylation Reactions with Norbornenes.[a]

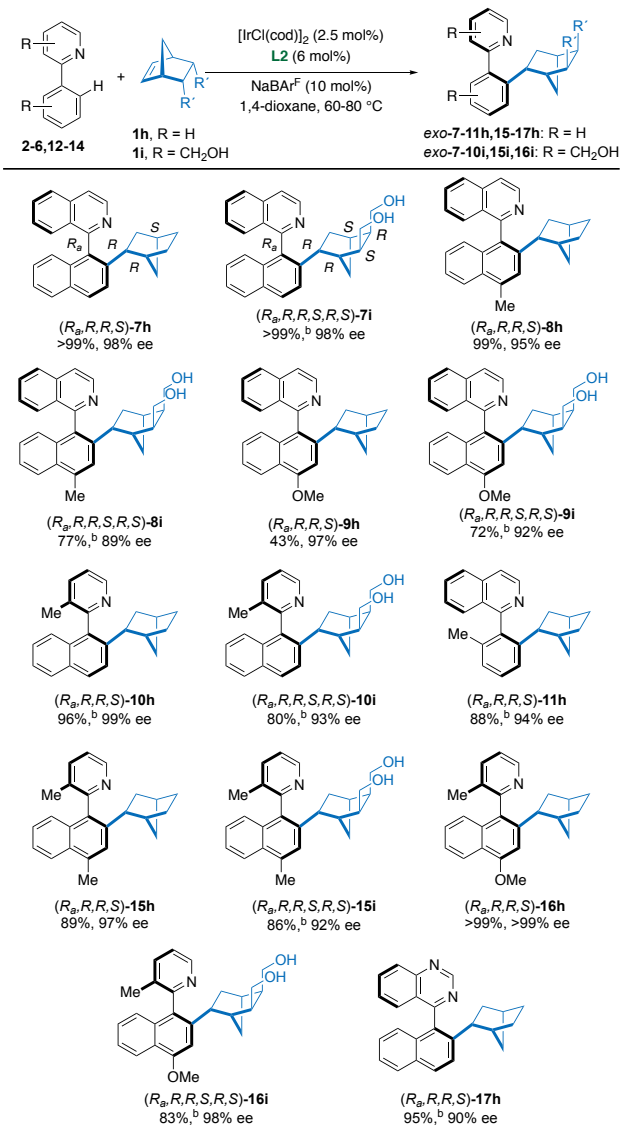

[a] Reactions performed on a 0.1 mmol scale using anhydrous 1,4-dioxane (1 mL/0.1 mmol **2-6**) and 5 equiv. of norbornene **1h**, for a 24 h period at 60 °C. Isolated yields after chromatography purification. *Exo/endo ratio* was determined by ^{1}H NMR in the crude reaction mixtures. Ee's determined by chiral HPLC analysis. [b] Reaction carried out at 80 °C for 24h.

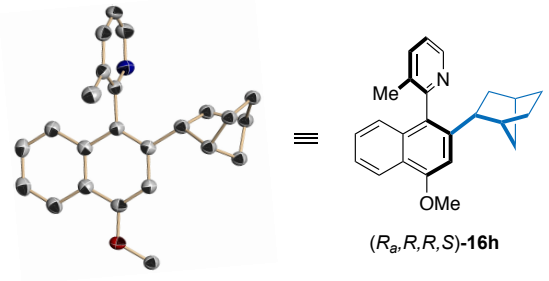

Figure 2. X-ray structure of (R_a,R,R,S) **16h** Thermal ellipsoids drawn at 50% probability. H atoms are omitted for clarity.

also performed at 1 mmol scale, affording **7h** in 98% yield and 97.5% ee, without compromising the *exo* selectivity.

Protecting group cleavage and representative transformations. The deprotection studies were initially carried out using *O*-benzyl derivative (S_a,R)-**7d** as the starting material (Scheme 2). Unexpectedly, C–O bond cleavage of this material either failed (H_2, Pd/C) or exclusively takes place at the secondary benzylic position (BBr_3 in DCM), despite the higher steric hindrance around the stereogenic center. Thus, reaction with BBr_3 afforded bromide **18** in 90% yield as a 85:15 diastereomeric mixture and with partial racemization. The observed epimerization–racemization process can be explained after formation of a cationic intermediate resulting from intramolecular nucleophilic displacement of the activated OBn fragment by the heterocyclic N atom, followed by nucleophilic attack of Br^-. A similar result was also observed for (S_a,R)-**7a**. The oxidative cleavage (DDQ in DCM) of the PMB group on (S_a,R)-**7e** afforded the desired free alcohol (S_a,R)-**19**, although in a poor 31% yield. Fortunately, cleavage of the MOM group of (S_a,R)-**7f** under acidic conditions (TfOH in DCM) could be satisfactorily accomplished to afford (S_a,R)-**19** in 75% yield without erosion of the enantiomeric purity. Under these conditions, other MOM derivatives **8f–10f** were also transformed into alcohols (S_a,R)-**20–22** in good to excellent yields and high ee´s. *Importantly, the hydroarylation–MOM deprotection sequence can be performed at 1 mmol scale to afford* (S_a,R)-**19** *a in better yield (77% isolated overall yield) and without erosion of the enantioselectivity.* Alcohols (S_a,R)-**19** and (S_a,R)-**22** are useful intermediates: nucleophilic substitution with diphenylphosphoryl azide (DPPA) takes

Scheme 2. Protecting Group Cleavage and Representative Transformations.

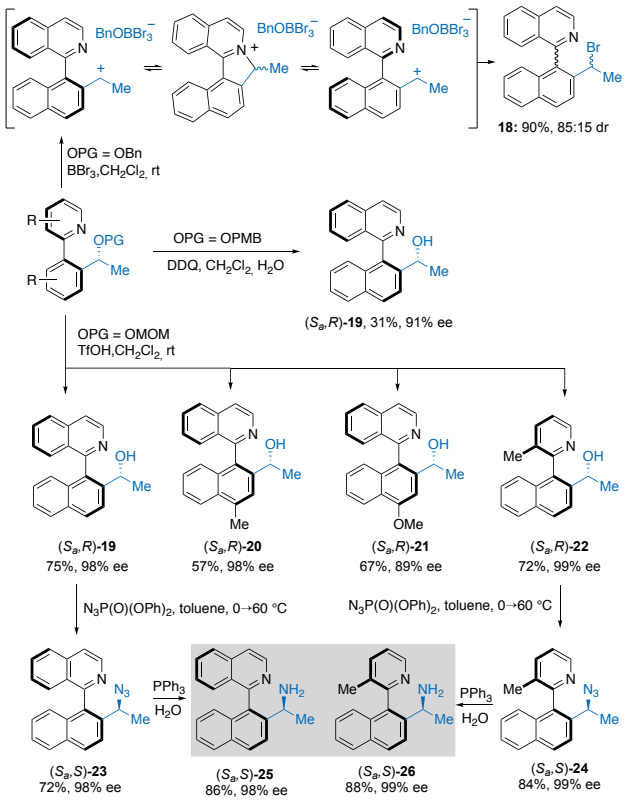

place with inversion of configuration to afford azides (S_a,S)-**23**,**24** in good yields, and subsequent Staudinger reduction efficiently afforded appealing diamines (S_a,S)-**25**,**26**.[18]

Kinetic isotope effect. Deuterium labelling experiments were carried out to gain mechanistic insight into the catalytic cycle. Two parallel hydroarylations of *n*-butyl vinyl ether **1a** were performed, one with the non-deuterated substrate **2** and the other with the deuterated counterpart **2′** (Scheme 3). An apparent KIE (K_D/K_H) value of ~0.9 was measured from the analysis of the reaction crudes after 4 h at 80 °C. On the other hand, the analysis of the deuterium incorporation in the recovered starting material **2′** (only ~22% D from ~99%) and the formed product (S_a,R)-**7′** (~46% D) showed a significant amount of hydrogen incorporation, revealing that the C–H activation and insertion steps are reversible. Although a correct value of the KIE cannot be provided by this data,[19] these experiments indicate that the C–H activation is not the rate determining step, and suggest that the migratory insertion should be the regio and stereodetermining step.

Scheme 3. KIE and Deuterium Labelling Experiments.

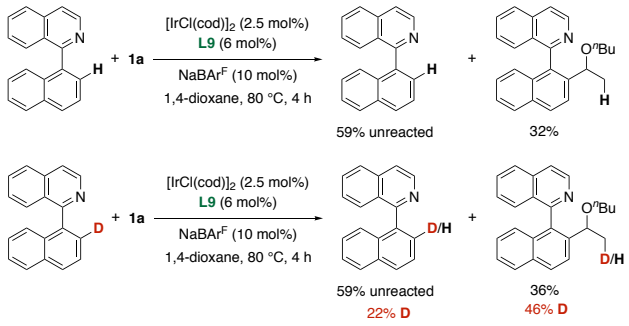

Computational studies. Theoretical calculations (ωB97xD / 6-31g(d,p) + SDD in 1,4-dioxane -SMD-; see the SI) have been carried out to rationalize the origin of the observed regio- and enantioselectivities and support the conclusions from the observed deuterium labelling experiments. While recent mechanistic studies on metal-catalyzed hydroarylation justify the regio- and central enantioselectivity of similar hydroarylation reactions.[20,21] in this research we also account for the extra complexity introduced by simultaneous generation of axial and central chirality. In line with related investigations, the reaction proceeds through a modified Chalk-Harrod-type mechanism,[22] with selectivity-determining migratory insertion into the Ir–C_{Aryl} bond preceding C–H reductive elimination. Also, regiocontrol is determined by the alkoxy group, that directs insertion so that the aryl group is coupled to the carbon *a* to it. The origin of diastereoselectivity is however more complex, and calculations suggest a cooperative effect of the BINAP, the heterobiaryl ligands and vinyl ether ligands, in which dispersive interactions play an important role.

Initial C–H oxidative addition of N-coordinated naphtylpyridine **5** to Ir^I is facile when assisted by vinyl ether, which is placed trans to hydride in the resulting Ir(III) complexes (see $\mathbf{B}_{H\text{-}t\text{-}vinyl}$ in Scheme 4). Up to eight octahedral isomers may result from this step, differentiated by the relative orientation of the double bond and by the configuration of the stereogenic axis. Importantly, dynamic kinetic resolution conditions are met at this stage, given the low epimerization barriers (*ca*. 15 kcal·mol^{-1}) that interconvert the R_a and S_a diastereomeric intermediates via C–C rotation.[8f,23] Then the following diastereomeric transition states should have different energy barriers to account for the observed enantioselectivity. Calculations of alkene migratory insertion into the Ir–C_{Aryl} bond of isomers $\mathbf{B}_{H\text{-}t\text{-}vinyl}$ yield barriers above 30 kcal·mol^{-1} (see the SI), as expected from the *trans* influence of the hydride ligand and could not explain the experimental enantioselectiviy. Thus, the remaining octahedral intermediates resulting from rearrangement of the BINAP, heterobiaryl, hydrido and vinyl ether ligands around the metal (Scheme 4) have also been considered in the calculations as

Scheme 4. Computational Study of C–H Oxidative Addition.[a]

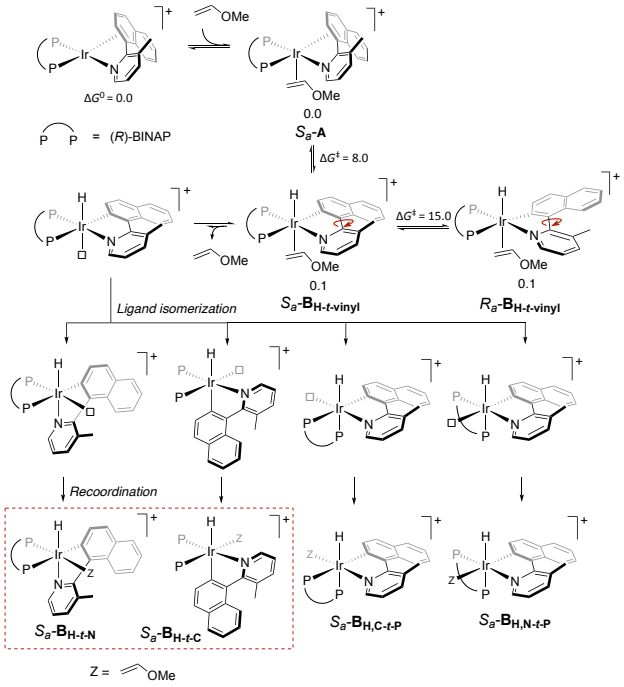

[a]Energies from [(BINAP)Ir(I)(5)]$^+$ + methyl vinyl ether in kcal·mol^{-1} and set of isomers considered in this study. Isomers in a dashed rectangle yield the lowest energy pathways for hydroarylation.

Scheme 5. Set of Diastereomers Considered for Geometric Isomer $\mathbf{B}_{H\text{-}t\text{-}N}$.[a]

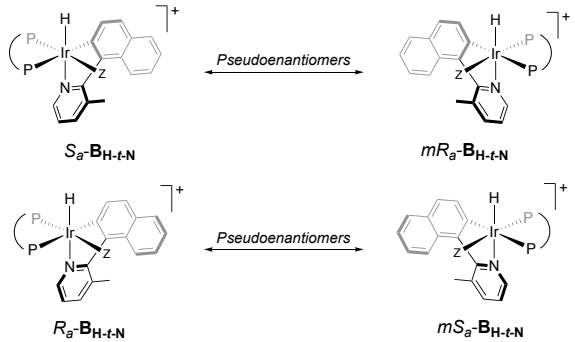

[a]The numbering of intermediates, e.g. $\mathbf{S_a}$-$\mathbf{B}_{H\text{-}t\text{-}N}$, comprises one capital letter (a sequence of intermediates in a given pathway type is assigned letters in alphabetical order), followed by a sequence of characters associated to the isomeric rearrangement of the first complex in any given pathway (i.e. H-*t*-N = "hydride trans to nitrogen"). The prefixes S_a and R_a relate to the configuration of the C–C axis of the heteroaryl ligand, whereas the *m* prefix refers to pseudo mirror image nature of a given isomer.

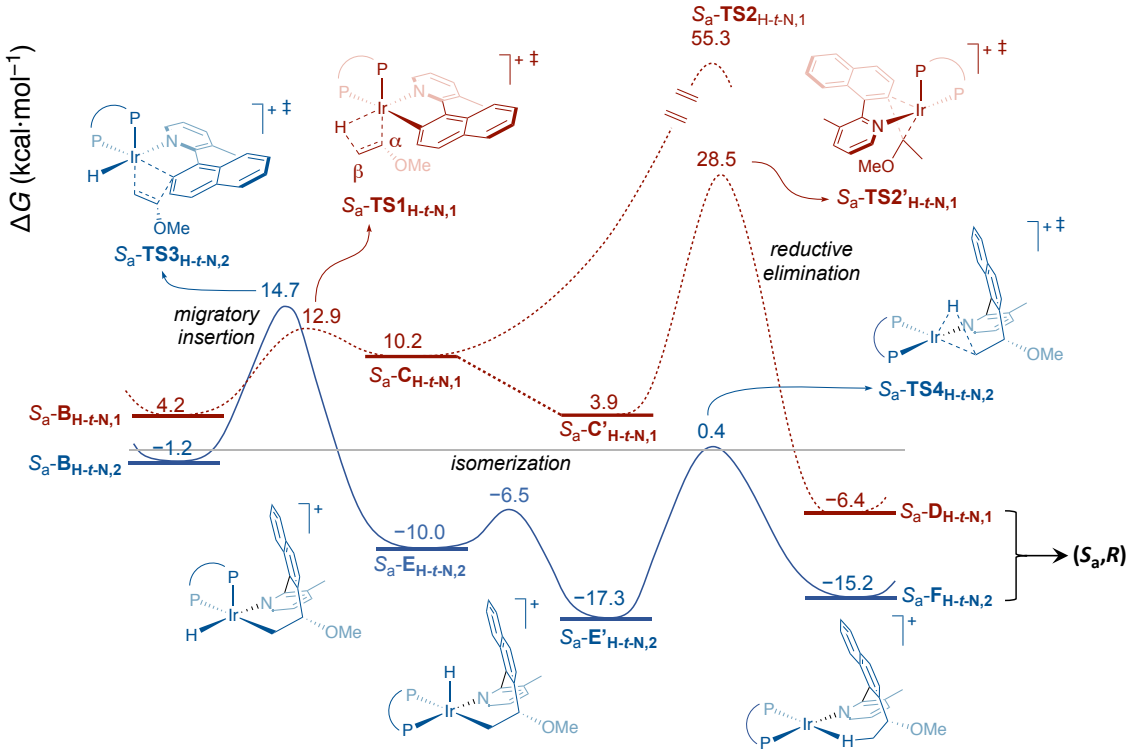

Figure 3. Free energy profiles for the formation of the (S_a,*R*) hydroarylation product via migratory insertion into Ir-H/C-C reductive elimination (red-dotted trace) and via insertion into Ir-C/C-H reductive elimination (blue solid trace) from isomers $\boldsymbol{S_a}$-$\mathbf{B_{H\text{-}t\text{-}N}}$.

starting points of the reaction manifold.[24] For the shake of clarity the following paragraphs will describe only pathways originating from the **H-*t*-N** set of diastereomers (Scheme 5), since these justify the experimental enantioselectivity having the lowest energy barriers. Results from calculations on alternative pathways starting from **H-*t*-C** diastereomers are also in accord with the experiments and can be found in the supplementary information, while the remaining reaction pathways originating in **H,C-*t*-P** and **H,N-*t*-P** isomers have high energy barriers that are at odds with the experimental conditions. Specifically, we will focus on relevant aspects of reaction pathways leading to branched (S_a,*R*) product, which is the major isomer seen in the experiments for linear vinyl ethers, and we will compare those to alternative pathways yielding linear or minor diastereomeric forms of branched products.Double bond insertion into either the Ir–H or Ir–C_{Aryl} bonds of the alkene complex $\boldsymbol{S_a}$-$\mathbf{B_{H\text{-}t\text{-}N}}$ and the ensuing pathways to hydroarylation are closed by C–C or C–H reductive elimination steps, respectively. These reaction sequences are examples of what has been described as Chalk-Harrod and modified-Chalk-Harrod type mechanisms.[21] In the first case, insertion into the Ir-H bond of the alkene complex $\boldsymbol{S_a}$-$\mathbf{B_{H\text{-}t\text{-}N,1}}$[25] has an overall barrier from [(BINAP)Ir(I)(**S**)]$^+$ + methyl vinyl ether of 12.9 kcal·mol^{-1} (Figure 3, red-dotted trace), whereas the reverse elementary step, β-elimination, requires only 2.7 kcal·mol^{-1} from $\boldsymbol{S_a}$-$\mathbf{C_{H\text{-}t\text{-}N,1}}$, in agreement with the reversibility of the insertion step. On the contrary, C–C reductive coupling to afford the (S_a,*R*) hydroarylation product from the insertion intermediate is inaccessible, since the step has an energy barrier ($\boldsymbol{S_a}$-$\mathbf{TS2_{H\text{-}t\text{-}N,1}}$) of more than 50 kcal·mol^{-1}. This may be a consequence of the C–H β-agostic interaction between the newly formed alkyl ligand and the metal in intermediate **C**, which is retained in the transition state **TS2**, constraining its geometry (Figure SC1). $\boldsymbol{S_a}$-$\mathbf{C_{H\text{-}t\text{-}N,1}}$ can however undergo facile isomerization through a trigonal bipyramidal transition state to a new species, $\boldsymbol{S_a}$-$\mathbf{C'_{H\text{-}t\text{-}N,1}}$, with N trans to phosphorous, from which C–C reductive coupling has an overall barrier of 28.5 kcal·mol^{-1}.[26] These results are entirely consistent with the literature[19,20] and will not be discussed in further detail. It should however be emphasized that they illustrate pathways for hydrogen-deuterium scrambling that are consistent with the deuteration experiments, since migratory insertion into Ir-H is fast and reversible, regardless of the high energy barrier found for C–C reductive coupling.

Regarding the second type of mechanism mentioned above, when double bond migratory insertion into the Ir–C_{Aryl} bond of $\boldsymbol{S_a}$-$\mathbf{B_{H\text{-}t\text{-}N,2}}$ (Figure 3, blue-solid trace) was calculated, it was found to be slightly more difficult than insertion into Ir–H in the previous route, having an energy barrier of 15.8 kcal·mol^{-1}. Then, similarly to the previous route, the insertion intermediate, $\boldsymbol{S_a}$-$\mathbf{E_{H\text{-}t\text{-}N,2}}$, undergoes almost barrier-less isomerization to place the biaryl N trans to phosphorous. This step is exergonic and yields a stable new intermediate, $\boldsymbol{S_a}$-$\mathbf{E'_{H\text{-}t\text{-}N,2}}$, which renders the overall step sequence irreversible ($\Delta G^{\ddagger}$= 32.0 kcal·mol^{-1}). However, reductive C–H coupling from this point on the way to the (S_a,*R*) product is relatively fast with a barrier of 17.7 kcal·mol^{-1}, at variance with C–C coupling in the previous pathway. Similar results have been found for alternative routes starting from other isomers of intermediates **B**, as can be seen in the supplementary information, which confirms a preference for a modified Chalk-Harrod-type mechanism in this reaction. In addition, these results are consistent with migratory insertion into Ir-C being the stereo-determining step.

The origin of the regioselectivity for this reaction is illustrated by the insertion of vinyl methyl ether into the Ir–C_{Aryl} bonds of $\boldsymbol{S_a}$-$\mathbf{B_{H\text{-}t\text{-}N,2}}$ and $\boldsymbol{S_a}$-$\mathbf{B_{H\text{-}t\text{-}N,3}}$, both alkene complexes being differentiated

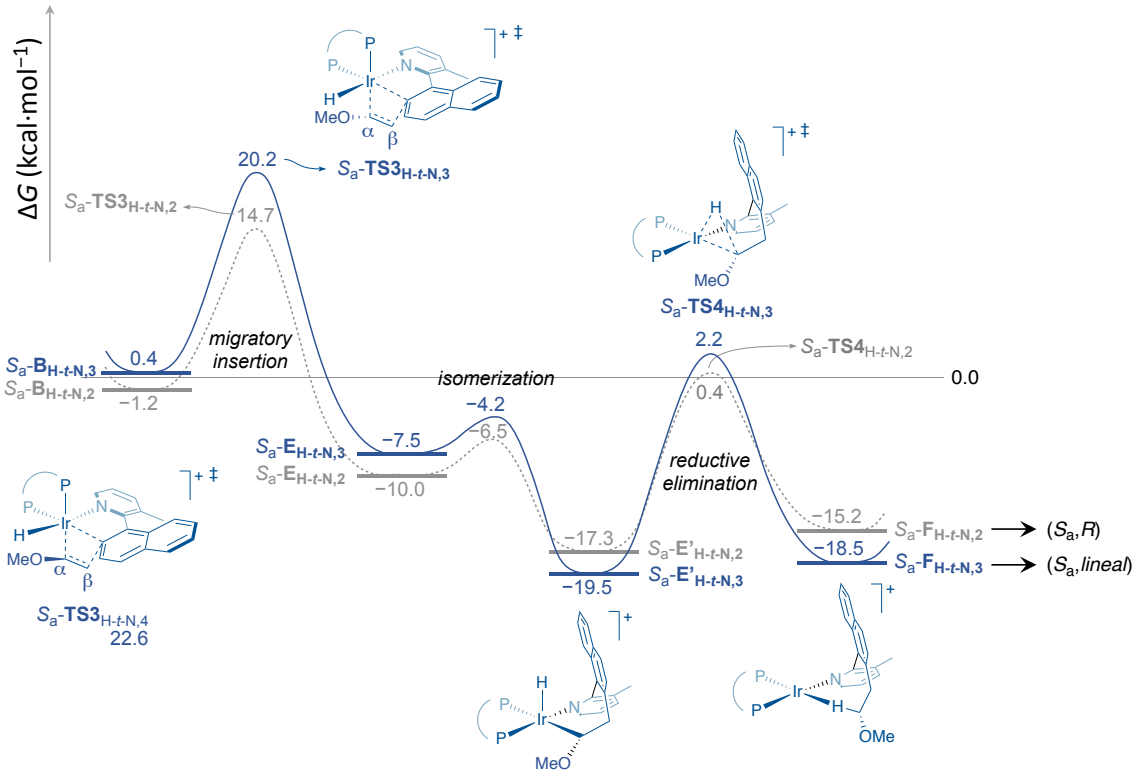

Figure 4. Free energy profiles for the formation of the branched (S_a,R) and (S_a,*linear*) hydroarylation products via migratory insertion into Ir–C_{Aryl}, C–H reductive elimination.

only by the orientation of the vinyl ether double bond. Thus, while α-insertion at ***S*$_a$-B$_{H\text{-}t\text{-}N,2}$** leads, as already shown, to the (S_a,R) product through an energy barrier of 15.8 kcal·mol^{-1}, the barriers for β-insertion at ***S*$_a$-B$_{H\text{-}t\text{-}N,3}$** and ***S*$_a$-B$_{H\text{-}t\text{-}N,4}$**, leading in both cases to the (S_a,*linear*) product, are 4.4 and 6.7 kcal·mol^{-1} higher respectively (Figure 4). Similar preference for α-insertion into Ir–C_{Aryl} has been found in routes starting from different isomers of **B**, and this is in line with related findings in the literature.[20,27] These results can be rationalized as resulting from the electron donating character of the alkoxy group, that stabilizes the transition state for migratory insertion (**TS3**) with the electrophilic iridium attaching to the least substituted carbon. That is, it favors C–C coupling with the carbon *α* to the alkoxy leading to branched product.

The origin of the enantioselectivity in this system is complex and can be ascribed to at least three contributions, the more conspicuous being that the energy barrier for migratory insertion into the Ir-C_{Aryl} bond depends on the configuration of the stereogenic axis relative to the vinyl ether in octahedral complexes **B**. Two more subtle, but determining contributions involve the orientation of the methoxide moiety and the presence of dispersive interactions between the chiral phosphine and the biaryl that may stabilize the stereo determining transition state. Regarding the first contribution, while ***S*$_a$-B$_{H\text{-}t\text{-}N,2}$** features the Ir-C_{Aryl} carbon pointing to the α carbon of the vinyl ether, in ***R*$_a$-B$_{H\text{-}t\text{-}N,2}$**, the corresponding diastereomer bearing the R_a form of the biaryl ligand, the Ir-C_{Aryl} carbon points away from it (Figure SC2). As a consequence, the transition state for migratory insertion into the Ir-C_{Aryl} bond of the latter, eventually leading to the (R_a,R) product, ***R*$_a$-TS3$_{H\text{-}t\text{-}N,2}$**, is severely distorted and lies 31.7 kcal·mol^{-1} above the origin, compared to 15.8 kcal·mol^{-1} for ***S*$_a$-TS3$_{H\text{-}t\text{-}N,2}$**. Scheme 6 summarizes the information gathered from the calculations for α-migratory insertion of vinyl ethers into the Ir-C_{Aryl} of the different diastereomers **H-*t*-N**, confirming the effect of the configuration of the stereogenic axis on the energy barriers. Inspection of these results reveal four routes with almost parallel energy profiles (see the SI) and energy barrier values for migratory insertion into Ir–C_{Aryl} that are within an interval of less than 2 kcal·mol^{-1} (from 17.1 to 15.3 kcal·mol^{-1}). Interestingly, the two most stable transition states (for the methyl vinyl ether containing model), ***S*$_a$-TS3$_{H\text{-}t\text{-}N,2}$** ($\Delta G^{\ddagger}$ = 15.8 kcal·mol^{-1}) and ***mR*$_a$-TS3$_{H\text{-}t\text{-}N,2}$** ($\Delta G^{\ddagger}$= 15.3 kcal·mol^{-1}) feature the methoxy group positioned in an *endo* fashion relative to the biaryl ligand, and the same is true for routes starting from isomers **H-*t*-C** (See the SI). This suggests a, perhaps counterintuitive, role for dispersive (attractive) interaction between the alkoxy moiety of the vinyl ether and the biaryl. However, this model system predicts the (R_a,S) isomer as the major product of the reaction, instead of the (S_a,R), as observed in the experimental study for linear OR groups. The small size of the methoxy moiety may not be able to account for the steric effects resulting from the larger alkoxy groups used in the experiments. Therefore, when OMe was replaced by the bulkier OCy fragment (i.e. the new model uses substrate **1b**) the calculations predict that the route leading to the (S_a,R) product has the most stable transition state for insertion into Ir–C_{Aryl}, ***S*$_a$-TS3$_{H\text{-}t\text{-}N,2,Cy}$** ($\Delta G^{\ddagger}$= 14.8 kcal·mol^{-1}), thus reproducing the experimental selectivity. Noncovalent interaction analysis (NCI)[28] of the two most stable transition states for the cyclohexylvinyl ether (**1b**)-containing system confirmed the presence of dispersive interactions between the endo-facing OCy moiety and the biaryl ligand, and a larger *π*-*π* interaction surface between the biaryl and the BINAP in the most favorable transition state[29] (Figure 5 and SC10), thus revealing a role for the chiral phosphine in the enantioselectivity control.[30]

Scheme 6. Geometries of Cationic Transition States for Migratory Insertion into Ir-C_{Aryl} Bonds.[a]

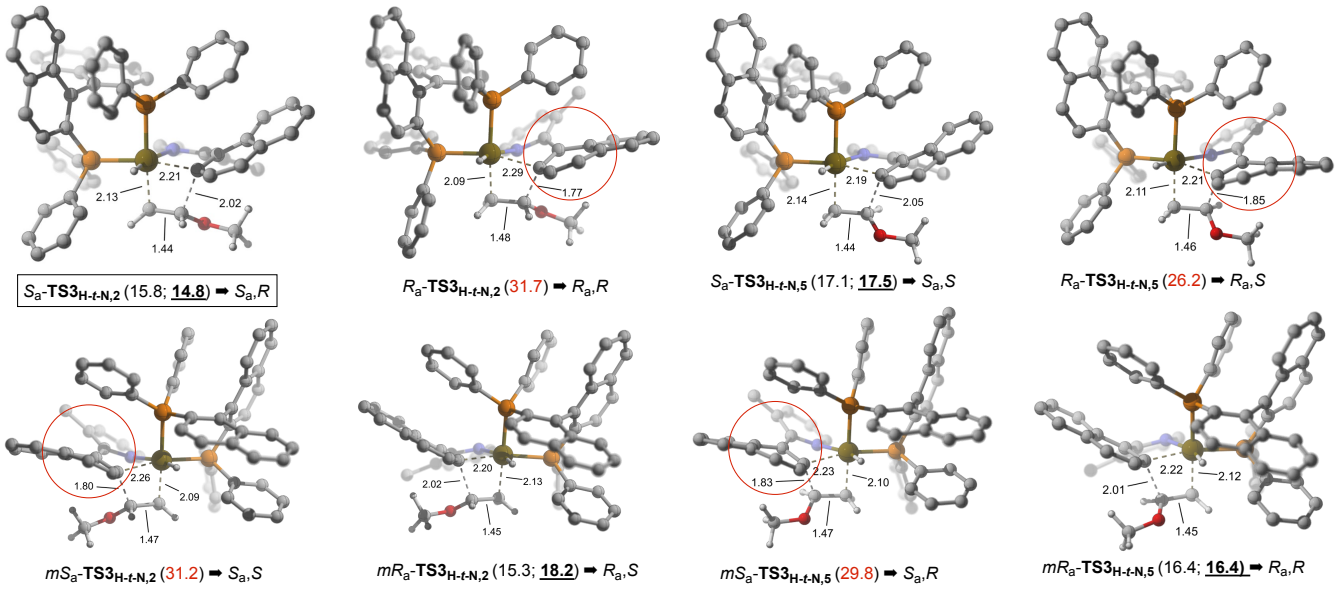

[a] Figures in parentheses correspond to Gibbs energies in kcal·mol^{-1} for R = Me and Cy (underlined). High-energy transition states are associated with severe distortions of the aryl moiety (highlighted with red circles).

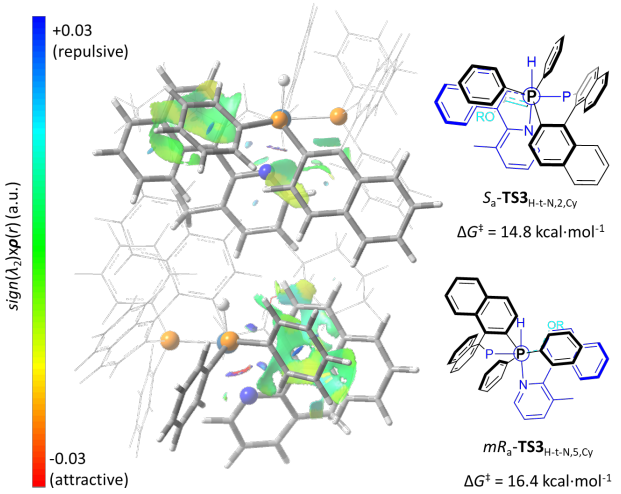

Figure 5. View along the P–Ir–C_{vinyl} axis of ***S*$_a$-TS3$_{H\text{-}t\text{-}N,2,Cy}$** and **m*R*$_a$-TS3$_{H\text{-}t\text{-}N,5,Cy}$**, showing the match/mismatch alignment of the biaryl and BINAP ligands: no interaction surface was located between the pyridyl fragment and BINAP in **m*R*$_a$-TS3$_{H\text{-}t\text{-}N,5,Cy}$**. The color code for the NCI plots is red = attractive / blue = repulsive. Green regions correspond to weak, van der Waals-type interactions (only relevant surfaces are shown for clarity).

CONCLUSIONS

In summary, a highly regio-, diastereo- and enantioselective (up to >20:1 dr, up to 99% ee) desymmetrization of configurationally labile heterobiaryls takes place through Ir-catalyzed hydroarylation of vinyl ethers or bicycloalkenes. The reaction affords appealing functionalized heterobiaryls with simultaneous installation of central and axial chirality. Deuterium labeling experiments together with computational studies suggest that the reaction proceeds via a modified Chalk-Harrod-type mechanism, and that the migratory insertion into the Ir–C_{Aryl} bond is the selectivity-determining step. The computational results are in fair agreement with the observed regioselectivity and absolute configuration.

ASSOCIATED CONTENT

Supporting Information. Experimental procedures and characterization data for new compounds, crystallographic data for (S_a,R)-**9b**, (R_a,S)-**7g** and (R_a,R,R,S) **16h**, and HPLC traces for compounds **7-11, 15-17**. Additional computational details. XYZ coordinates of calculated species. This material is available free of charge via the Internet at http://pubs.acs.org.

AUTHOR INFORMATION

Corresponding Authors

*ffernan@us.es
*joaquin.lopez@iiq.csic.es
*abel.ros@iiq.csic.es
*jmlassa@iiq.csic.es

ORCID

Antonio Romero-Arenas: 0000-0002-0605-5091
Valentín Hornillos: 0000-0002-6181-9146
Javier Iglesias-Sigüenza: 0000-0001-8846-2303
Rosario Fernández: 0000-0002-1755-1525
Joaquín López-Serrano: 0000-0003-3999-0155
Abel Ros: 0000-0002-3455-5675
José M. Lassaletta: 0000-0003-1772-2723

ACKNOWLEDGMENT

We thank the Spanish Ministerio de Ciencia e Innovación (Grants CTQ2013-48164-C2-1-P, CTQ2013-48164-C2-2-P and CTQ2016-75193-P, contract RYC-2013-12585 for A.R., contract RYC-2017-22294 for V. H.), European FEDER Funds, and Junta de Andalucía (Grant 2012/FQM 10787) for financial support. The use of computational facilities of the Centro de Servicios de Informática y Redes de

Comunicaciones (CSIRC), Universidad de Granada and the Supercomputing Centre of Galicia (CESGA) is gratefully acknowledged.

REFERENCES

(1) (a) Kozlowski, M. C.; Morgan, B. J.; Linton, E. C. Total synthesis of chiral biary natural products by asymmetric biaryl coupling**.** *Chem. Soc. Rev.* **2009**, *38*, 3193-3207. (b) Bringmann, G.; Gulder, T.; Gulder, T. A. M.; Breuning, M. Atroposelective total synthesis of axially chiral biaryl natural products. *Chem. Rev.*, **2011**, *111*, 563-639.

(2) (a) Tang, W.; Zhang, X. New chiral Phosphorus ligands for enantioselective hydrogenation. *Chem. Rev.* **2003**, *103*, 3029-3070. (b) Canac, Y.; Chauvin, R. Atropochiral C,X- and C,C-Chelating Carbon Ligands. *Eur. J. Inorg. Chem*. **2010**, *16*, 2325-2335. (c) *Apropisomerism and Axial Chirality*; Lassaletta, J. M. Ed.; Word Scientific: New Jersey, 2019.

(3) (a) Loxq, P.; Manoury, E.; Poli, R.; Deydier, E.; Labande, A. Synthesis of axially chiral biaryl compounds by asymmetric catalytic reactions with transition metals. *Coord. Chem. Rev.* **2016**, *308*, 131–190 and references cited therein. For selected references to see: (b) Egami, H.; Matsumoto, K.; Oguma, T.; Kunisu, T.; Katsuki, T. Enantioenriched synthesis of C_1-symmetric BINOLs: Iron-catalyzed cross-coupling of 2-naphthols and some mechanistic insight. *J. Am. Chem. Soc.* **2010**, *132*, 13633-13635. (c) Narute, S.; Parnes, R.; Toste, F. D; Pappo, D. Enantioselective oxidative homocoupling and cross-coupling of 2-naphthols catalyzed by chiral iron phosphate complexes. *J. Am. Chem. Soc.* **2016**, *138*, 16553-16560. (d) Bermejo, A.; Ros, A.; Fernández, R.; Lassaletta, J. M. C_2-symmetric bis-hydrazones as ligands in the asymmetric Suzuki–Miyaura Cross-coupling. *J. Am. Chem. Soc.* **2008**, *130*, 15798-15799. (e) Uozumi, Y.; Matsuura, Y.; Arakawa, T.; Yamada, Y. M. A. Asymmetric Suzuki–Miyaura coupling in water with a chiral Palladium catalyst supported on an amphiphilic resin. *Angew. Chem., Int. Ed.* **2009**, *48*, 2708-2710. (f) Shen, X.; Jones, G. O.; Watson, D. A.; Bhayana, B.; Buchwald, S. L. Enantioselective synthesis of axially chiral biaryls by the Pd-catalyzed Suzuki–Miyaura reaction: Substrate scope and quantum mechanical investigations. *J. Am. Chem. Soc*. **2010**, *132*, 11278-11287. (g) Yamamoto, T.; Akai, Y.; Nagata, Y.; Suginome, M. Highly enantioselective synthesis of axially chiral biarylphosphonates: asymmetric Suzuki-Miyaura coupling using high-molecular-weight, helically chiral polyquinoxaline-based phosphines**.** *Angew. Chem. Int. Ed.* **2011**, *50*, 8844-8847. (h) Ros, A.; Estepa, B.; Bermejo, A.; Álvarez, E.; Fernández, R.; Lassaletta, J. M. Phosphino hydrazones as suitable ligands in the asymmetric Suzuki–Miyaura cross-coupling. *J. Org. Chem***. 2012**, *77*, 4740-4750. (i) Wang, S.; Li, J.; Miao, T.; Wu, W.; Li, Q.; Zhuang, Y.; Zhou, Z.; Qiu, L. Highly efficient synthesis of a class of novel chiral-bridged atropisomeric monophosphine ligands via simple desymmetrization and their applications in asymmetric Suzuki-Miyaura coupling reaction. *Org. Lett.*, **2012**, *14*, 1966-1969. (j) Shen, D.; Xu, Y.; Shi**,** S.-L. A bulky chiral N-heterocyclic carbene Palladium catalyst enables highly enantioselective Suzuki-Miyaura cross-coupling reactions for the synthesis of biaryl atropisomers. *J. Am. Chem. Soc.* **2019**, *141*, 14938-14945.

(4) (a) Amatore, M.; Auber, C. Recent advances in stereoselective [2+2+2] cycloadditions. *Eur. J. Org. Chem*. **2015**, 265-286 and references cited therein.

(5) (a) Shirakawa, S.; Liu, S.; Kaneko, S. Organocatalyzed asymmetric synthesis of axially, planar, and helical Chiral Compounds**.** *Chem. Asian J*, **2016**, *11*, 330-341 and references cited therein. For selected references to see: (b) Li, G.-Q.; Gao, H.; Keene, C.; Devonas, M.; Ess, D. H.; Kürti, L. Organocatalytic aryl–aryl bond formation: An atroposelective [3,3]-rearrangement approach to BINAM derivatives. *J. Am. Chem. Soc.* **2013**, *135*, 7414-7417. (c) Chen, Y.-H.; Cheng, D.-J.; Zhang, J.; Wang, Y.; Liu, X.-Y.; Tan, B. Atroposelective synthesis of axially chiral biaryldiols via organocatalytic arylation of 2-naphthols**.** *J. Am. Chem. Soc.* **2015**, *137*, 15062-15065. (d) Zhang, H.-H.; Wang, C.-S.; Li, C.; Mei, G.-J.; Li, Y.; Shi, F. Design and enantioselective construction of axially chiral naphthyl-indole skeletons. *Angew. Chem. Int. Ed*. **2017**, *56*, 116-121.

(6) (a) Wencel-Delord, J.; Panossian, A.; Leroux, F. R.; Colobert, F. Recent advances and new concepts for the synthesis of axially stereoenriched biaryls. *Chem. Soc. Rev*. **2015**, *44*, 3418-3430 and references cited therein. (b) Yu, C.; Huang, H.; Zhang, Y.; Wang, W. Dynamic kinetic resolution of biaryl lactones via a chiral bifunctional amine thiourea-catalyzed highly atropo-enantioselective transesterification. *J. Am. Chem. Soc*. **2016**, *138*, 6956-6959. (c) Mori, K.; Itakura, T.; Akiyama, T. Enantiodivergent atroposelective synthesis of chiral biaryls by asymmetric transfer hydrogenation: Chiral phosphoric acid catalyzed dynamic kinetic resolution. *Angew. Chem. Int. Ed.* **2016**, *55*, 11642-11646. (d) Zhang, J.; Wang J., Atropoenantioselective redox-neutral amination of biaryl compounds through borrowing hydrogen and dynamic kinetic resolution. *Angew. Chem. Int. Ed.* **2018**, *57*, 465-469. (e) Gustafson, J.; Lim, D.; Miller, S. J. Dynamic kinetic resolution of biaryl atropisomers via peptide-catalyzed asymmetric bromination. *Science* **2010**, *328*, 1251-1255. (f) Gao, D.-W.; Gu, Q.; You, S.-L. Pd(II)-catalyzed intermolecular direct C–H bond iodination: An efficient approach toward the synthesis of axially chiral compounds via kinetic resolution. *ACS Catal.* **2014**, *4*, 2741-2745. (g) Hazra, C. K.; Dherbassy, Q.; Wencel-Delord, J.; Colobert, F. Synthesis of axially chiral biaryls through sulfoxide-directed asymmetric mild C-H activation and dynamic kinetic resolution. *Angew. Chem. Int. Ed*. **2014**, *53*, 13871-13875. (h) Yao, Q.-J.; Zhang, S.; Zhan, B.-B.; Shi, B.-F. Atroposelective synthesis of axially chiral biaryls by Palladium-catalyzed asymmetric C-H olefination enabled by a transient chiral auxiliary. *Angew. Chem. Int. Ed*. **2017**, *56*, 6617-6621. (i) Sun, Q.-Y.; Ma, W.-Y.; Yang, K.-F.; Cao, J.; Zheng, Z.-Z.; Xu, Z.; Cui, Y.-M.; Xu, L.-W. Enantioselective synthesis of axially chiral vinyl arenes through palladium-catalyzed C–H olefination. *ChemCommun.* **2018**, *54*, 10706-10709. (j) Zhao, K.; Duan, L.; Xu, S.; Jiang, J.; Fu, Y.; Gu, Z. Enhanced reactivity by torsional strain of cyclic diaryliodonium in Cu-catalyzed enantioselective ring-opening reaction. *Chem*, **2019**, *4*, 599-612. (k) Deng, R.; Xi, J.; Li, Q.; Gu, Z. Enantioselective carbon-carbon bond cleavage for biaryl atropisomers synthesis. *Chem*, **2019**, *5*, 1834-1846. (l) Liao, G.; Zhou, T.; Yao, Q.-J.; Shi, B.-F. Recent advances in the synthesis of axially chiral biaryls via transition metal-catalysed asymmetric C–H functionalization. *Chem. Commun*. **2019**, *55*, 8514–852.

(7) Ros, A.; Ramírez, P.; Fernández, R.; Lassaletta, J. M. Asymmetric Synthesis of Axially Chiral Biaryls and Heterobiaryls. Chapter 1. in Atropisomerism and Axial Chirality, World Scientific Publishing Co., New Jersey, 2019.

(8) (a) Ros, A.;L Estepa, B.; Ramírez-López, P.; Álvarez, E.; Fernández, R.; Lassaletta, J. M. Dynamic kinetic cross-coupling strategy for the asymmetric synthesis of axially chiral heterobiaryls. *J. Am. Chem. Soc*. **2013**, *135*, 15730–15733. (b) Ramírez-López, P.; Ros, A.; Estepa, B.; Fernández, R.; Fiser, B.; Gómez-Bengoa, E.; Lassaletta, J. M. A dynamic kinetic C–P cross–coupling for the asymmetric synthesis of axially chiral P,N ligands. *ACS Catal*. **2016**, *6*, 3955–3964. (c) Bhat, V.; Wang, S.; Stoltz, B. M.; Virgil, S. C. Asymmetric synthesis of QUINAP via dynamic kinetic resolution. *J. Am. Chem. Soc.* **2013**, *135*, 16829–16832. (d) Ramírez-López, P.; Ros, A.; Romero-Arenas, A.; Iglesias-Sigüenza, J.; Fernández, R.; Lassaletta, J. M. Synthesis of IAN-type N,N-ligands via dynamic kinetic asymmetric Buchwald–Hartwig amination. *J. Am. Chem. Soc*. **2016**, *138*, 12053–12056. (e) Hornillos, V.; Ros, A.; Ramírez-Lopez, P.; Iglesias-Sigüenza, J.; Fernandez, R.; Lassaletta, J. M. Synthesis of axially chiral heterobiaryl alkynes *via* dynamic kinetic asymmetric alkynylation**.** *Chem. Commun*., 2016, *52*, 14121–14124. (f) Carmona, J. A., Hornillos, V.; Ramírez-López, P.; Ros, A.; Iglesias-Sigüenza, J.; Gómez-Bengoa, E.; Fernández, R.; Lassaletta, J. M. Dynamic kinetic asymmetric Heck reaction for the simultaneous generation of central and axial chirality. *J. Am. Chem. Soc*. **2018**, *140*, 11067–11075.

(9) Swamy, T.; Reddy, B. V. S.; Grée, R.; Ravinder, V. Substrate-Directed C–H Functionalization of 2-ArylPyridines by Transition Metal Complexes. *ChemistrySelect* **2018**, *3*, 47–70.

(10) Kakiuchi, F.; Gendre, P. L.; Yamada, A.; Ohtaki, H.; Murai, S. Atropselective alkylation of biaryl compounds by means of transition metal-catalyzed C–H/olefin coupling. *Tetrahedron: Asymmetry*, **2000**, *11*, 2647–2651.

(11) Zheng, J.; You, S.-L. Construction of axial chirality by Rhodium-catalyzed asymmetric dehydrogenative Heck coupling of biaryl compounds with alkenes. *Angew. Chem. Int. Ed.* **2014**, *53*, 13244–13247.

(12) Zheng, J.; Cui, W.-J.; Zheng, C.; You, S.-L. Synthesis and application of chiral spiro Cp ligands in Rhodium-catalyzed asymmetric oxidative

coupling of biaryl compounds with alkenes. *J. Am. Chem. Soc.* **2016**, *138*, 5242–5245.
(13) Wang, Q.; Cai, Z.-J.; Liu, C.-X.; Gu, Q.; You S.-L. Rhodium-Catalyzed Atroposelective C–H Arylation: Efficient Synthesis of Axially Chiral Heterobiaryls. *J. Am. Chem. Soc.* **2019**, *141*, 9504–9510.
(14) Ros, A.; Estepa, B.; López-Rodríguez, R.; Álvarez, E.; Fernández, R.; Lassaletta, J. M. Use of hemilabile N,N ligands in nitrogen-directed Iridium-catalyzed borylations of arenes. *Angew. Chem. Int. Ed.* **2011**, *50*, 11724–11728.
(15) (a) Ebe, Y.; Nishimura, T. Iridium-catalyzed branch-selective hydroarylation of vinyl ethers via C–H bond activation. *J. Am. Chem. Soc.* **2015**, *137*, 5899–5902. (b) Ebe, Y.; Onoda, M.; Nishimura, T.; Yorimitsu, H. Iridium-catalyzed regio- and enantioselective hydroarylation of alkenyl ethers by olefin isomerization. *Angew. Chem. Int. Ed.* **2017**, *56*, 5607–5611.
(16) Zhu, S.-F.; Zhou, Q.-L. Chiral Spiro Ligands in Privileged Chiral Ligands and Catalysts; Zhou, Q.-L., Ed.; Wiley-VCH: Weinheim, 2011; chapter 4, p 13–170. (b) Xie, J.-H.; Zhou, Q.-L. Chiral Diphosphine and Monodentate Phosphorus Ligands on a Spiro Scaffold for Transition-Metal-Catalyzed Asymmetric Reactions. *Acc. Chem. Res.* **2008**, *41*, 581–593. (c) Xie, J.-H.; Zhou, Q.-L. Magical Chiral Spiro Ligands. *Acta Chim. Sinica* **2014**, *72*, 778)
(17) This anomaly is attributed to the push-pull conjugation with the OMe group in the Ir(III) intermediates formed after C–H activation. A similar behavior has been observed in Pd(II) complexes formed after oxidative addition of heterobiaryl electrophiles. See ref. 8e.
(18) This methodology is complementary to the previously described atroposelective zinc-catalyzed hydrosilylation of heterobiaryl ketones, which afforded the diastereomeric alcohols (R_a,R)-**19,20,22**: Hornillos, V.; Carmona, J. A.; Ros, A.; Iglesias-Sigüenza, J.; López-Serrano, J.; Fernández, R.; Lassaletta, J. M. Dynamic kinetic resolution of heterobiaryl ketones by Zinc-catalyzed asymmetric hydrosilylation. *Angew. Chem. Int. Ed.* **2018**, *57*, 3777–3781.
(19) (a) Gómez-Gallego, M.; Sierra, M. A. Kinetic Isotope Effects in the Study of Organometallic Reaction Mechanisms. *Chem. Rev.* **2011**, *111*, 4857–4963. (b) Simmons, E. M.; Hartwig, J. F. On the Interpretation of Deuterium Kinetic Isotope Effects in C-H Bond Functionalizations by Transition- Metal Complexes. *Angew. Chem. Int. Ed.* **2012**, *51*, 3066–3072. (c) Sevov. C. S.; Hartwig, J. F. Iridium-Catalyzed Intermolecular Asymmetric Hydroheteroarylation of Bicycloalkenes. *J. Am. Chem. Soc.* **2013**, *135*, 2116–2119.
(20) For selected recent examples see: (a) Zhanga, M.; Huang. G. Mechanism of iridium-catalysed branched selective hydroarylation of vinyl ethers: a computational study. *Dalton Trans.* **2016**, *45*, 3552–3557. (b) Huang, G.; Liu, P. Mechanism and Origins of Ligand-Controlled Linear Versus Branched Selectivity of Iridium-Catalyzed Hydroarylation of Alkenes. *ACS Catal.* **2016**, *6*, 809–820. (c) Azpíroz, R.; Giuseppe, D.-G.; Urriolabeitia, A.; Passarelli, V.; Polo, V.; Pérez-Torrente, J. J.; Oro, L. A.; Castarlenas. R. Hydride–Rhodium(III)-N-Heterocyclic Carbene Catalyst for Tandem Alkylation/Alkenylation via C–H Activation. *ACS Catal.* **2019**, *9*, 9372–9386.
(21) Zhang, M.; Hu, L.; Lang, Y.; Cao, Y.; Huang. G. Mechanism and Origins of Regio- and Enantioselectivities of Iridium-Catalyzed Hydroarylation of Alkenyl Ethers. *J. Org. Chem.* **2018**, *83*, 2937–2947.
(22) (a) Chalk, A. J.; Harrod, J. F. Homogeneous Catalysis. I. Double Bond Migration in n-Olefins, Catalyzed by Group VIII Metal Complexes. *J. Am. Chem. Soc.* **1965**, *87*, 16–21. (b) Sakaki, S.; Sumimoto, M.; Fukuhara, M.; Sugimoto, M.; Fujimoto, H.; Matsuzaki, S. Why Does the Rhodium-Catalyzed Hydrosilylation of Alkenes Take Place through a Modified Chalk–Harrod Mechanism? A Theoretical Study. *Organometallics* **2002**, *21*, 3788–3802. (c) Sevov, C. S.; Zhou, J. (S.); Hartwig. J. F. Iridium-Catalyzed, Intermolecular Hydroamination of Unactivated Alkenes with Indoles. *J. Am. Chem. Soc.* **2014**, *136*, 3200–3207. (d) Torigoe, T.; Ohmura, T.; Suginome. M. Asymmetric Cycloisomerization of o-Alkenyl-N-Methylanilines to Indolines by Iridium-Catalyzed C(sp^3)–H Addition to Carbon–Carbon Double Bonds. *Angew. Chem. Int. Ed.* **2017**, *56*, 14272–14276.
(23) (a) Ramírez-López, P.; Ros, A.; Estepa, B.; Fernández, R.; Fiser, B.; Gómez-Bengoa, E.; Lassaletta. J. M. A Dynamic Kinetic C–P Cross–Coupling for the Asymmetric Synthesis of Axially Chiral P,N Ligands. *ACS Catal.* **2016**, *6*, 3955–3964.
(24) Ligand rearrangements from $\mathbf{A_{H\text{-}\textit{t}\text{-}vinyl}}$ to give isomers $\mathbf{A_{H\text{-}\textit{t}\text{-}N}}$, $\mathbf{A_{H\text{-}\textit{t}\text{-}C}}$ and $\mathbf{A_{H,N\text{-}\textit{t}\text{-}P}}$ have energy barriers below 20 kcal·mol^{-1}. These results are estimates since only rearrangements on pentacoordinate species have been explored. No barrier was found for $\mathbf{A_{H,C\text{-}\textit{t}\text{-}P,}}$ however this species lies 22.9 kcal·mol^{-1} above the common origin of energies.
(25) The number (1-8) added to after the comma refers to the orientation of the double bond of the vinylether in the initial adduct.
(26) Species $\boldsymbol{S_a}$-$\mathbf{C'_{H\text{-}\textit{t}\text{-}N,1}}$ is closely related to an intermediate of the route starting from $\boldsymbol{S_a}$-$\mathbf{B_{H\text{-}\textit{t}\text{-}C,1,}}$ which also features reversible migratory insertion into Ir-H through a barrier of 16.1 kcal·mol^{-1} (See Figure SC3).
(27) von Schenck, H.; Åkermark, B.; Svensson. M. Electronic Control of the Regiochemistry in the Heck Reaction. *J. Am. Chem. Soc.* **2003**, *125*, 3503–3508.
(28) Johnson, E. R.; Keinan, S.; Mori-Sánchez, P.; Contreras-García, J.; Cohen, A. J.; Yang. W. Revealing Noncovalent Interactions. *J. Am. Chem. Soc.* **2010**, *132*, 6498–6506.
(29) Salomó, E.; Gallen, A.; Sciortino, G.; Ujaque, G.; Grabulosa, A.; Lledós, A.; Riera A.; Xavier Verdaguer. X. Direct Asymmetric Hydrogenation of N-Methyl and N-Alkyl Imines with an Ir(III)H Catalyst. *J. Am. Chem. Soc.* **2018**, *140*, 16967–16970.
(30) Some authors (see reference 19 for example) suggest that the Ir-C_β–C_α–C_{Aryl} dihedral angle at the transition state for migratory insertion into Ir–C_{Aryl} can be correlated with the corresponding energy barrier, since large values of the dihedral imply distorted transition states deviated from the expected planar geometry. In our case, there is no correlation between the energy barrier and the value of the dihedral at **TS3**: $\boldsymbol{S_a}$-$\mathbf{TS3_{H\text{-}\textit{t}\text{-}N,2,Cy,}}$ −17.3°; $\mathbf{m}\boldsymbol{R_a}$-$\mathbf{TS3_{H\text{-}\textit{t}\text{-}N,2,Cy,}}$ −20.6°; $\boldsymbol{S_a}$-$\mathbf{TS3_{H\text{-}\textit{t}\text{-}N,5,Cy,}}$ 2.8°; $\boldsymbol{R_a}$-$\mathbf{TS3_{H\text{-}\textit{t}\text{-}N,5,Cy,}}$ 6.3°.

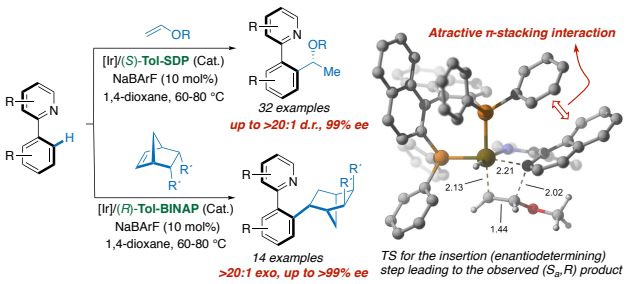
OR
[Ir]/(S)-Tol-SDP (Cat.)
NaBArF (10 mol%)
1,4-dioxane, 60-80 °C
32 examples
up to >20:1 d.r., 99% ee
[Ir]/(R)-Tol-BINAP (Cat.)
NaBArF (10 mol%)
1,4-dioxane, 60-80 °C
14 examples
>20:1 exo, up to >99% ee
Atractive π-stacking interaction
2.13
2.21
2.02
1.44
TS for the insertion (enantiodetermining) step leading to the observed (Sa,R) product